Structure and Stability of Monomeric .lambda. Repressor: NMR Evidence for Two-State Folding

ARTICLE *in* BIOCHEMISTRY · APRIL 1995

Impact Factor: 3.02 · DOI: 10.1021/bi00012a003 · Source: PubMed

2 AUTHORS:

Guewha S. Huang
Hokan Life Technology, Taiwan
60 PUBLICATIONS **1,653** CITATIONS
SEE PROFILE

Terrence Gilbert Oas
Duke University Medical Center
79 PUBLICATIONS **4,743** CITATIONS
SEE PROFILE

Structure and Stability of Monomeric λ Repressor: NMR Evidence for Two-State Folding†

Guewha Steven Huang and Terrence G. Oas*

Department of Biochemistry, Duke University Medical Center, Durham, North Carolina 27710

Received January 20, 1995; Revised Manuscript Received February 10, 1995®

ABSTRACT: The absence of equilibrium intermediates in protein folding reactions (i.e., two-state folding) simplifies thermodynamic and kinetic analyses but is difficult to prove rigorously. We demonstrate a sensitive method for detecting partially folded species based on using proton chemical shifts as local probes of structure. The coincidence of denaturation curves for probes throughout the molecule is a particularly stringent test for two-state folding. In this study we investigate a new form of the N-terminal domain of bacteriophage λ repressor consisting of residues 6−85 (λ_{6-85}) using nuclear magnetic resonance (NMR) and circular dichroism (CD). This truncated version lacks the residues required for dimerization and is monomeric under the conditions used for NMR. Heteronuclear NMR was used to assign the ^{1}H, ^{15}N, and backbone ^{13}C resonances. The secondary and tertiary structure of λ_{6-85} is very similar to that reported for the crystal structure of the DNA-bound 1−92 fragment [Beamer, L. J., and Pabo, C. O. (1992) *J. Mol. Biol. 227,* 177−196], as judged by analysis of chemical shifts, amide hydrogen exchange, amide−alpha coupling constants, and nuclear Overhauser enhancements. Thermal and urea denaturation studies were conducted using the chemical shifts of the four aromatic side chains as local probes and the CD signal at 222 nm as a global probe. Plots of the fraction denatured versus denaturant concentration obtained from these studies are identical for all probes under all conditions studied. This observation provides strong evidence for two-state folding, indicating that there are no populated intermediates in the folding of λ_{6-85}.

Small globular proteins are useful models for studying the thermodynamics of protein folding (Dill & Shortle, 1991). In many cases, the denaturation of these proteins has been described as a two-state process involving the interconversion of only native and fully denatured conformations. In this situation, partially folded intermediates are not observed because they are significantly less stable than the native and denatured states (Murphy et al., 1992; Schellman, 1987). Two-state folding is the result of the highly cooperative interactions that stabilize the folded state (Creighton, 1993) and the tendency to minimize exposed hydrophobic surface area (Murphy et al., 1992).

Although the two-state model describes denaturation of many proteins correctly, other models can correctly predict the sigmoidal shape of the denaturation curve (Dill & Shortle, 1991). More rigorous criteria for establishing a two-state transition have been described (Jackson & Fersht, 1991): (1) the coincidence of denaturation curves derived from different physical properties; (2) the lack of evidence of significant intermediate populations; (3) equivalent calorimetric and van't Hoff enthalpies (Privalov & Khechinashvili, 1974); and (4) equivalent kinetic and thermodynamic estimates of the apparent free energy of denaturation (ΔG_{app}) and its denaturant dependence.

There are several reasons to develop a model system that displays two-state folding behavior. First, in proteins with complex folding pathways (e.g., rearrangement of disulfide bonds, domain−domain interactions, proline isomerization) it is difficult to describe the thermodynamics of denaturation. To characterize the energetics of folding, a simple system is needed. Second, the interpretation of folding kinetics is greatly simplified in a two-state system, allowing the determination of rate constants from relaxation times. Third, as pointed out by Lattman and Rose (1993), two-state folding implies that even under destabilizing conditions, or in the presence of mildly destabilizing mutations, the small population of folded protein adopts a native-like conformation. Therefore, the conformation of such a protein is independent of its stability and is dictated by the overall sequence rather than by specific local interactions.

Most physical probes of protein structure monitor change in either overall conformation or the environment of a specific part of the protein. For example, circular dichroism spectropolarimetry (CD)[1] in the far-ultraviolet is sensitive to global secondary structure, and fluorescence is sensitive to the local environments of tryptophan residues. It has long been recognized that the nuclear magnetic resonance (NMR) chemical shift is sensitive to environment (Wüthrich, 1986). Because the environment of a residue in the native state differs from that in the denatured state, the same residue has different chemical shifts in these two states. If exchange between the native and denatured states occurs at a frequency much faster than this difference in chemical shift, only a single resonance will be observed, and the apparent chemical shift is the population-weighted average of the native and denatured chemical shifts (Wemmer et al., 1981). When folding is two state and the two states are in fast exchange, the fraction of protein in each state can be extracted from the chemical shifts. In principle, the denaturation curve for each residue can be determined. Under these conditions,

† This work supported by NIH Grant GM45322.

* To whom correspondence should be addressed: Box 3711; E-mail, oas@bchm.biochem.duke.edu; telephone, (919) 684-4363; FAX, 684-8885.

® Abstract published in *Advance ACS Abstracts,* March 15, 1995.

0006-2960/95/0434-3884$09.00/0

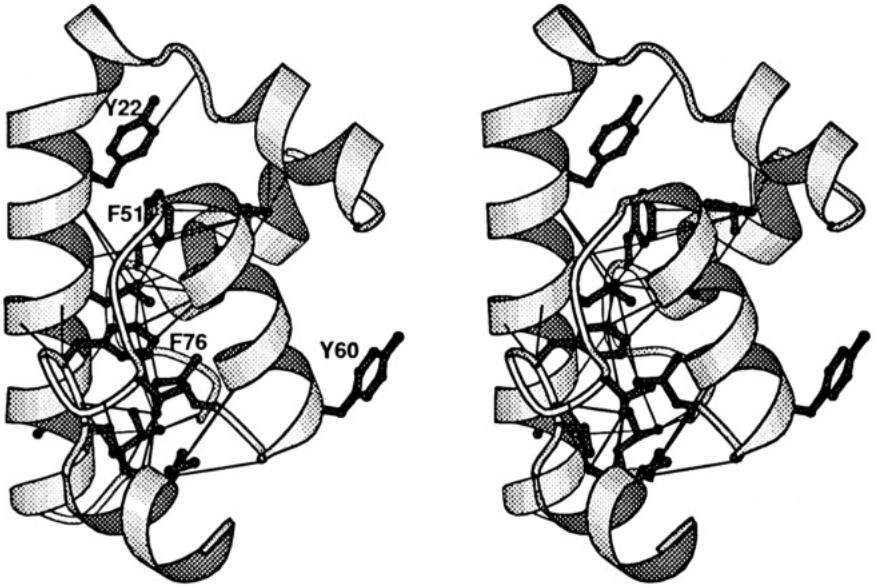

FIGURE 1: Stereoview of λ_{6-85} with coordinates from the protein−DNA cocrystal structure of Beamer and Pabo (1992). Side chains of Tyr22, Phe51, Tyr60, and Phe76 are indicated. Lines indicate unambiguous long-distance NOEs between heavy atoms. Figure made with MOLSCRIPT (Kraulis, 1991).

the structure of the whole protein can be monitored by NMR throughout the folding transition, and each resonance is a separate test of the two-state model.

We have applied this approach to study the folding of the N-terminal domain of λ repressor (Sauer et al., 1990). The crystal structure of the protein−DNA complex is known to 1.8 Å resolution (Beamer & Pabo, 1992; Jordan & Pabo, 1988). The protein comprises five helices with loops or turns to form a single hydrophobic core [Figure 1; for review see Sauer (1990)]. This system is attractive because a large number of core variants have been constructed and characterized (Lim et al., 1992; Lim & Sauer, 1989, 1991; Sauer et al., 1990).

The ^{1}H chemical shifts of all the aromatic resonances of λ repressor N-terminal domain have been determined using a combination of isotopic labeling and site-directed mutagenesis (Weiss et al., 1984). This domain is designated λ_{1-102} because it is a fragment consisting of the first 102 residues. Under the conditions of the NMR experiments, the protein dimerizes with a dissociation constant (K_d) of 0.3 mM (Weiss et al., 1987b). As deduced from analysis of the NMR data, the dimerization interface involves residues in helix 5. Further assignment was hampered by oligomerization of the protein. The dimer−monomer exchange process broadens the ^{1}H NMR spectrum, making it difficult to assign using homonuclear methods (Weiss et al., 1987a).

Intermolecular contacts are made between residues 81 and 91′, 84 and 91′, 85 and 88′, 87 and 87′, and 88 and 88′ in the crystal structures (Beamer & Pabo, 1992; Pabo & Lewis, 1982; Weiss et al., 1987a). Residues 81, 84, and 87 are intolerant to replacement by other amino acids, confirming their role in dimerization (Reidhaar-Olson & Sauer, 1990). To overcome dimerization-induced line broadening, in this study we use a truncated version (Wendell Lim, personal communication) of the N-terminal domain, designated λ_{6-85}. This new version of λ repressor lacks the dimerization interface and the first five amino acids [disordered in solution (Jordan & Pabo, 1988; Weiss et al., 1984)] and was designed to create a monomeric protein without disrupting the hydrophobic core. This was confirmed by the similarity in the CD spectra of λ_{6-85} and λ_{1-102}. In addition, the thermal denaturation of λ_{6-85} monitored by the CD signal at 222 nm has a T_m of 55 °C which is nearly identical to that of λ_{1-102} (55.7 °C), indicating a similar stability for both proteins (Lim et al., 1992). The new version presumably does not bind DNA because it lacks the N-terminal arm which contributes to DNA-binding affinity (Eliason et al., 1985) and because λ_{1-102} binds DNA exclusively as the dimer (Weiss et al., 1987b). Here we use the truncated version, λ_{6-85}, to demonstrate the utility and potential of NMR as a tool for studying equilibrium thermodynamics of protein folding.

MATERIALS AND METHODS

Expression and Purification of λ_{6-85}. Plasmid pWL300 containing the gene encoding residues 6−85 of λ repressor cloned into the T7 expression vector (Studier et al., 1990) pAED4 (Doering, 1992), the generous gift of Wendell Lim. The gene was expressed in *Escherichia coli* strain BL21-(DE3), induced with 0.4 mM IPTG. The purification protocol is a modification of one used previously for other versions of λ repressor (Lim et al., 1992). For a typical 1 L

[1] Abbreviations: CD, circular dichroism spectropolarimetry; CSI, chemical shift index; DQF-COSY, double-quantum-filtered correlated spectroscopy; EDTA, ethylenediaminetetraacetic acid; HPLC, high-performance liquid chromatography; HMQC, heteronuclear multiple-quantum coherence spectroscopy; HSQC, heteronuclear single-quantum coherence spectroscopy; IPTG, isopropyl β-D-thiogalactopyranoside; $^3J_{HN\alpha}$, scalar amide−α coupling constant; K_d, dissociation constant for dimer; k_{obs}, rate constant for amide proton exchange rate; k_{int}, intrinsic exchange rate constant; m, denaturant dependence of ΔG_{app}; NMR, nuclear magnetic resonance spectroscopy; NOE, nuclear Overhauser enhancement; NOESY, nuclear Overhauser enhancement and exchange spectroscopy; PF, protection factor; F_d, fraction denatured; R, universal gas constant; T_m, the temperature at which the denatured population equals the native population; TMSP, 3-(trimethylsilyl)propionic acid sodium salt; TOCSY, total correlated spectroscopy; δ, chemical shift; $\Delta\delta$, change in chemical shift upon denaturation; ΔC_p, heat capacity of denaturation; ΔG_0, ΔG_{app} in the absence of denaturant; ΔG_{app}, apparent free energy of denaturation; λ_{1-92}, the first 92 residues of λ repressor; λ_{1-102}, the first 102 residues of λ repressor; λ_{6-85}, residues 6−85 of λ repressor with the replacement of Pro6 by Ser and Tyr85 by Arg; 1D, 2D, and 3D, one, two, and three dimensional.

scale preparation, the cell lysate (in 40 mL TE, pH 8.0), from a French press, was loaded onto a 60-mL DEAE-Sephacel (Pharmacia) column equilibrated with 50 mM KCl, 10 mM Tris (pH 8.0), 2 mM $CaCl_2$, 0.1 mM EDTA, and 5% glycerol. The eluent was dialyzed against 10 mM KCl, 20 mM potassium acetate, pH 5.0, and 5% glycerol using Spectra/Por dialysis tubing. The dialysate was applied to a 15-mL Affi-Gel blue (Bio-Rad) column equilibrated with the same buffer and was eluted with a linear 10−200 mM KCl gradient. The major peak, as detected by absorbance at 280 nm, was further purified by reverse-phase HPLC with a C-18 column (Vydac) in acetonitrile/water/0.1% trifluoroacetic acid. To produce uniformly ^{15}N labeled protein, expression was carried out in minimal media (Farmer et al., 1992) supplemented with 1 g/L $^{15}NH_4Cl$ (Isotec Inc., 99% ^{15}N). For $^{15}N/^{13}C$ double labeling, 2 g/L [^{13}C]glucose (Isotec Inc., 97% ^{13}C) was used as the sole carbon source. More than 95% isotope incorporation was achieved, as judged by electrospray mass spectrometry (data not shown).

Size Exclusion Chromatography. Size exclusion chromatography was used to determine the oligomeric state of λ_{6-85} under NMR conditions. A poly(hydroxyethyl) HPLC column (PolyLC Inc.) was preequilibrated with NMR buffer (10% D_2O, 10 mM CD_3COOD, 100 mM NaCl, 17 μg/mL TMSP, 1 mM NaN_3, pH 5.6) with a flow rate of 0.5 mL/min. The protein was dissolved in NMR buffer at a concentration of 3.8 mM [λ_{1-102} behaves as a dimer under these conditions (Weiss et al., 1987b)] and injected onto the column. The molecular mass standards (Sigma) were aprotinin (6.5 kDa), cytochrome c (12.4 kDa), carbonic anhydrase (29 kDa), and bovine serum albumin (66 kDa).

NMR Spectroscopy. NMR samples consisted of 2−3 mM protein in 0.6 mL of NMR buffer. Urea denaturation experiments were performed using a 500-MHz Varian Unity spectrometer. All other NMR experiments were conducted using a 600-MHz Varian Unity spectrometer. Data were processed with FELIX software (Biosym, Inc.).

DQF-COSY (Rance et al., 1983; Shaka & Freeman, 1983), TOCSY (Braunschweiler & Ernst, 1983; Davis & Bax, 1985), and NOESY (Macura & Ernst, 1980) spectra were acquired at 30 °C with a spectral width of 6500 Hz in each dimension. Proton chemical shifts were referenced to TMSP at −0.015 ppm (de Marco, 1977). TOCSY spectra were acquired with a 150-ms mixing time. NOESY spectra were acquired with mixing times of 80 and 150 ms. Quadrature detection was accomplished by the method of States et al. (1981).

Heteronuclear experiments were acquired at 30 °C. $^{15}N-^{1}H$ HSQC, HMQC-COSY, HMQC-NOESY, HMQC-TOCSY (Gronenborn et al., 1989), gradient-enhanced 3D ^{15}N-HMQC-NOESY (Vuister et al., 1992), and gradient-enhanced ^{15}N HMQC-TOCSY spectra were acquired on a uniformly ^{15}N labeled sample. Refocused HNCA, HNCOCA, HNCO, and HNCACO were collected on a uniformly $^{13}C/^{15}N$ labeled sample (Farmer et al., 1992; Ikura et al., 1990). The ^{1}H sweep width was 6500 Hz, the ^{15}N sweep width was 1800 Hz, and the ^{13}C sweep width was 2700 Hz. ^{15}N chemical shifts were referenced to an external capillary containing 2.9 M $^{15}NH_4Cl$ in 1 M HCl (24.93 ppm relative to NH_3) (Levy & Lichter, 1979). ^{13}C chemical shifts were referenced relative to hypothetical TMSP (0 ppm) (Bax & Subramanian, 1986).

Amide Hydrogen Exchange. Amide hydrogen exchange rates were determined by following the reduction of the $^{15}N-^{1}H$ HSQC cross-peak volume in D_2O. ^{15}N-Labeled λ_{6-85} was initially dissolved to a concentration of ~3 mM in 0.6 mL of 100% H_2O, 10 mM CD_3COOD, 100 mM NaCl, 17 μg/mL TMSP, and 1 mM NaN_3 at the desired temperature and pH. Amide hydrogen exchange was initiated by centrifuging the protein solution through a 3-mL Sephadex G25 (Pharmacia) column preequilibrated with the same buffer made with D_2O at the experimental temperature. The first several spectra were acquired in 15 min. Spectra were then acquired at 30-min time intervals. First-order rate constants (k_{obs}) were obtained by fitting the data using KaleidaGraph (Synergy Software). Exchange experiments were performed under three different conditions: pH 5.6, 25 °C; pH 5.6, 4 °C; and pH 4.0, 4 °C. Protection factors were derived by dividing k_{obs} by k_{int}, the intrinsic exchange rate constant. The intrinsic rate constant for each amide in λ_{6-85} was calculated as described by Englander et al. (1972) using the correction table of Bai et al. (1993).

Amide−alpha *Coupling Constants.* Amide−alpha coupling constants ($^{3}J_{HN\alpha}$) were obtained by measuring the splitting of HMQC-COSY autopeaks in the ^{15}N (Forman-Kay et al., 1990). A total of 2000 increments in the F_1 dimension were acquired and zero-filled to 4096 points.

Thermal Denaturation. The buffer used in these experiments was 20 mM KD_2PO_4, 100 mM NaCl, 17 μg/mL TMSP, and 1 mM NaN_3, pH 8.0, in ~99% D_2O with 0, 1, or 2 M urea. Urea concentrations were determined by refractometry (Pace, 1986). The protein concentration was 100 μM. One-dimensional ^{1}H NMR spectra were collected as a function of temperature in 2 °C steps from 2 to 74 °C with 15-min equilibration prior to acquisition. A total of 1024 transients were taken for each temperature. NMR data were referenced to TMSP at each temperature.

The fraction of denatured state (F_d) was determined using the equation:

$$F_d = \frac{\delta - (a_1 + b_1 T)}{(a_2 + b_2 T) - (a_1 + b_1 T)} \quad (1)$$

where a_1 and b_1 are the intercept and slope of the temperature-dependent native state baseline and a_2 and b_2 are the intercept and slope of the temperature-dependent denatured state baseline. The native and denatured baselines were obtained using KaleidaGraph from unweighted nonlinear least squares fits of the chemical shift versus temperature curves to the equation:

$$\delta = \frac{(a_1 + b_1 T) + (a_2 + b_2 T)e^{(a_3 + b_3/T)}}{1 + e^{(a_3 + b_3/T)}} \quad (2)$$

In eq 2, it is assumed that the free energy of denaturation is a linear function of temperature [i.e., that $\Delta C_p = 0$ (Schellman, 1987)]. Although this is not the case, the assumption is sufficiently accurate to allow fits of the baselines so that eq 1 could be used to determine F_d vs temperature. In eq 2, a_3 represents the temperature-independent component of the equilibrium constant, and b_3 represents the temperature-dependent part. Because the actual value of ΔC_p cannot be determined accurately from spectroscopic denaturation curves

with similar T_m's (Privalov & Khechinashvili, 1974), we have not attempted to extract thermodynamic parameters from these data.

Thermal denaturation was also monitored with an AVIV/62DS spectropolarimeter under conditions identical to those used for NMR denaturation studies (including ~99% D_2O as solvent). A multiple cell holder was used to collect data for all urea concentrations simultaneously. The signal was averaged for 15 s for each sample in 1 °C steps. The temperature was allowed to equilibrate for 30 s prior to data collection at each temperature. Denaturation curves were fitted to eq 2, with ellipticity at 222 nm substituted for chemical shift. Thermal denaturations were ~70% reversible in 0 M urea, due to irreversible aggregation at high temperatures. In the presence of urea, denaturations were at least 90% reversible.

Urea Denaturation. Protein was dissolved in NMR buffer (~99% D_2O, 10 mM CD_3COOD, 100 mM NaCl, 17 μg/mL TMSP, 1 mM NaN_3, pH 5.6) at 50 μM with various concentrations of urea as determined by refractometry (Pace, 1986). Each sample was equilibrated at 37 °C for at least 20 min. A one-dimensional ^1H NMR spectrum (1024 transients) was acquired at each urea concentration. NMR data were referenced to TMSP for each urea concentration. Urea denaturation was also monitored by CD at 222 nm with a 60-s averaging time. The chemical shift and ellipticity were then fitted to the equation:

$$[\theta]_{222} \text{ or } \delta = \frac{(a + b[\text{urea}]) + (c + d[\text{urea}])e^{(-\Delta G_{app}/RT)}}{1 + e^{(-\Delta G_{app}/RT)}} \quad (3)$$

where a and b are the slope and intercept of the urea-dependent native state baseline, c and d are the slope and intercept of the urea-dependent denatured state baseline, and ΔG_{app} is the apparent free energy change of denaturation at a given urea concentration where

$$\Delta G_{app} = \Delta G_0 - m[\text{urea}] \quad (4)$$

In eq 4, ΔG_0 is the apparent free energy of the denaturation reaction at 37 °C in the absence of urea and m is the slope of the linear free energy urea dependence (Schellman, 1994).

RESULTS

The experimental approach of these studies was to (1) establish that λ_{6-85} is a homogeneous, monomeric system under the conditions of the study, (2) assign the NMR spectra of the molecule so as to allow structural characterization of the native state in solution, and (3) investigate the thermal and chemical denaturation behavior of the molecule with the aim of determining whether the system represents a good model system for further protein folding studies.

Oligomerization State. It is important to establish whether λ_{6-85} is monomeric under the conditions of these studies for two reasons. First, it is critical to establish that all NMR-based structural information (e.g., distance constraints) arises from intramolecular interactions. Second, molecular association/dissociation reactions can greatly complicate the interpretation of denaturation data. Two different experiments were performed to test the oligomerization state of λ_{6-85} at the concentrations required to perform NMR. At 3.8 mM, the protein (9 kDa) elutes on a poly(hydroxyethyl)

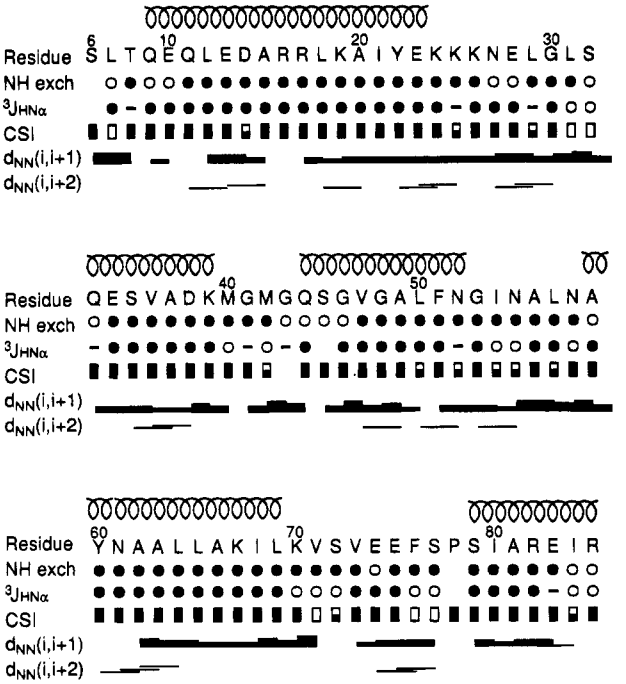

FIGURE 2: Summary of NMR evidence of secondary structure in λ_{6-85}. Helices in the crystal structure are indicated above the sequence (Beamer & Pabo, 1992). For amide exchange (NH), residues with protection factors >10 at pH 4, 4 °C, are indicated by filled circles. Scalar coupling constants ($^3J_{NH\alpha}$) are indicated by open circles (larger than 8 Hz), filled circles (less than 6 Hz), and dashes (between 6 and 8 Hz). Chemical shift indices (Wishart et al., 1991, 1992) are indicated by open rectangles (+1), half-filled rectangles (0), filled rectangles (−1), or no symbol (+1 and −1; for the two Gly43 protons). NOEs are represented by thin bars (weak), medium bars, and thick bars (strong).

size exclusion column between aprotinin (6.5 kDa) and cytochrome c (12.4 kDa) as expected for the monomeric species. One-dimensional ^1H NMR spectra at 50 μM, 0.5 mM, and 3 mM are identical (data not shown), indicating that there is no conformational change over this concentration range. These results indicate that λ_{6-85} is a nonassociating monomer, as expected given the removal of the dimer interface.

NMR Assignments. Homonuclear 2D-TOCSY (Davis & Bax, 1985) spectra of λ_{6-85} show poor dispersion of $^1H_\alpha$ proton resonances. Poor $^1H_\alpha$ dispersion is typically observed for helical proteins, e.g., interleukin 4 (Powers et al., 1992). For this reason, sequential assignment was achieved using 3D through-bond connectivity experiments, i.e., HNCA, HNCO, HNCOCA, and HNCACO (Farmer et al., 1992; Ikura et al., 1990). After assignment of $^1H_\alpha$, ^{15}N, and backbone ^{13}C resonances, side-chain protons for each spin system were assigned by a combination of homonuclear DQF-COSY (Rance et al., 1983; Shaka & Freeman, 1983) and TOCSY (Braunschweiler & Ernst, 1983; Davis & Bax, 1985). Pro78 was assigned as the only spin system without an amide proton. The N-terminal Ser6 was assigned by NOE connection to Leu7 NH. ^1H, ^{15}N, and backbone ^{13}C assignments are listed in Table 1 of the supplementary material.

Secondary Structure. The secondary structure of λ_{6-85} was determined from protection factors, amide−alpha proton coupling constants ($^3J_{HN\alpha}$), chemical shift indices (CSIs), and unambiguous $NN_{(i,i+n)}$ NOEs, as shown in Figure 2. These parameters indicate the position of secondary structure in

the following ways: (1) Amide hydrogens involved in secondary structure tend to have protection factors greater than 10 (Bai et al., 1993). (2) $^3J_{HN\alpha}$ values below 6 Hz are indicative of helix and above 7 indicative of sheet (Wüthrich, 1986). (3) CSI values are obtained by comparing the observed H_α chemical shift to its corresponding random-coil chemical shift. Generally, H_α's in helices are shifted downfield by at least 0.1 ppm from the random-coil values (CSI = −1), and H_α's in sheets are shifted upfield by at least 0.1 ppm (CSI = 1). H_α's within ±0.1 ppm are given CSI values of 0 (Wishart et al., 1991, 1992). (4) $NN_{(i,i+n)}$ NOEs are indicative of α helix because the corresponding internuclear distances are long in sheets or extended structure (Wüthrich, 1986). The results summarized in Figure 2 are consistent with the positions of the α helices observed in the λ_{1-92} repressor−DNA cocrystal (Beamer & Pabo, 1992), depicted above the residue numbers.

In λ_{6-85}, helix 1 starts at Gln9, indicated by the low coupling constant (less than 4 Hz) and helical CSI (−1). The continuity of helix 1 is indicated by the consistently low coupling constants, helical CSIs, high protection factors, and NOEs between neighboring residues ($d_{NN(i,i+1)}$, $d_{NN(i,i+2)}$). Helix 1 ends at Glu24, as indicated by the nonhelical coupling constant (7.5 Hz) and nonhelical CSI (0 or +1) of Lys25. Helix 2 is delimited by a stretch of low coupling constants, helical CSIs, protected amides, and medium-range NOEs, starting at Gln33. The high coupling constant of Met40 (7.8 Hz) indicates a nonhelical conformation and marks the end of helix 2. Helix 3 starts at Gln44, as indicated by the helical coupling constant and CSI. The helix stops at Phe51 because Gly52 has a nonhelical coupling constant (6.6 Hz) and the percentage of helical CSI at this residue is lower than 75% for a window of four residues (from 49 to 52) (Wishart et al., 1992). Helix 4 starts at Asn60, as indicated by a stretch of helical coupling constants and CSIs starting from Asn60. It ends at Leu69, as judged by the high coupling constant at Lys70 (8.0 Hz). Helix 5 starts at Ser79 as indicated by low coupling constants, protected amides, and helical CSIs for residues 79−83. The protection factor, coupling constant, and CSI of Glu83 suggest that helix 5 ends at this residue. All nonhelical residues with protected amides participate in hydrogen bonds in the crystal structure except residues 57 and 58 (see below). In general, the data summarized in Figure 2 indicate that the secondary structure of λ_{6-85} in solution is identical to that observed for the same region of the dimer in the protein−DNA cocrystal (Beamer & Pabo, 1992).

Tertiary Structure. Thirty unambiguously assigned long-range NOEs from 2D-NOESY and ^{15}N-HSQC-NOESY are shown in Figure 1. These include NOEs involving aromatic side-chain residues, the methyl groups of Leu7, Leu18, Leu65, Val36, Val47, and Val73. Due to the poor dispersion in 2D-NOESY, most of the NOEs were determined from ^{15}N-HSQC-NOESY. The distances between protons corresponding to unambiguous NOEs were 5 Å or less in the cocrystal structure (Beamer & Pabo, 1992), indicating that the solution structure of λ_{6-85} is very similar. Figure 1 shows that the NOEs are distributed throughout the molecule. The observation of NOEs between core residues (e.g., Leu18 δCH_3 to Phe76 δH and Phe76 εH; Leu18 δCH_3 to Phe51 δH and Phe51 εH; Val47 γCH_3 to Phe51 δH, Phe51 εH, and Phe51 ζH) indicates that the core structure is maintained in λ_{6-85}. The observation of NOEs between different secondary structural units (e.g., Leu7 δCH_3 in helix 1 to NHs of Ala56 and Ala57 in the loop between helix 3 and helix 4) indicates the conservation of the overall fold.

Although the solution structure of λ_{6-85} is highly homologous to the crystal structure of the DNA complex, two observations suggest possible differences. First, residues 83, 84, and 85 (at the end of the fifth helix) have coupling constants of 7.4, 8.2, and 8.1 Hz with nonhelical CSIs. Residues 84 and 85 have fairly low protection factors (<10). Taken together, the NMR data indicate that residues 83−85 are probably not in a stable helical conformation. This is not surprising given that the original helix 5 has been cut in half. Nevertheless, the first four residues of the helix adopt a stable helical conformation despite this truncation. The second apparent difference involves the amide backbone protons of Leu57 and Asn58, which do not appear to form intramolecular hydrogen bonds in the cocrystal structure but are protected from hydrogen exchange in solution (protection factors > 100). This discrepancy may be the result of a conformation change in this region induced by DNA binding. Asn56 and Asn58 participate in hydrogen bonds to the phosphate backbone of the DNA in the cocrystal structure (Beamer & Pabo, 1992).

Thermal Denaturation. The four aromatic side chains in λ_{6-85} were used as local probes of unfolding: Tyr22, Phe51, Tyr60, and Phe76 (see Figure 1). These side chains are located in different regions of the molecule and probe different environments. Phe51 and Phe76 are buried, the aromatic ring of Tyr22 is partially buried, and the ring of Tyr60 is exposed to solvent. Thermal denaturations in 0, 1, and 2 M urea were performed from 2 to 74 °C and monitored by ^{1}H NMR. The aromatic regions of these spectra are shown in Figure 3. The chemical shift of each aromatic proton versus temperature was fitted to eq 2 to obtain the native and denatured baselines. The fitted parameters are listed in Table 2 of the supplementary material. The F_d versus temperature curves (eq 1) are shown in Figure 4. To simplify the figure, the F_d shown is the average for all protons within a given residue. Denaturation curves of the aromatic resonances are superimposable at each urea concentration.

An advantage of using chemical shift as a probe of folding is that it is insensitive to partial aggregation of the sample at elevated temperatures, a common problem in thermal denaturation studies. Figure 3 shows a loss of signal intensity, presumably due to aggregation, at high temperatures, particularly in the absence of urea. However, because aggregation is slow on the NMR time scale (halftime of ~30 min, at 70 °C, 0 M urea), the F_d calculated from the residual signal is unaffected by partial aggregation.

The thermal denaturation of λ_{6-85} was monitored by CD at 222 nm under the same conditions used for the NMR thermal denaturation experiments. The baselines for these curves were determined as described for the NMR data. The fitted parameters are listed in Table 2 of the supplementary material. Plots of F_d versus temperature are shown in Figure 4. The CD and NMR data are superimposable. The approximate T_m's obtained from the average denaturation curves at 0, 1, and 2 M urea are 55, 49, and 45 °C, respectively.

Urea Denaturation. The aromatic region of the ^{1}H NMR spectrum of 50 μM λ_{6-85} was acquired in 0−6.4 M urea at 37 °C, pH 5.6. Tyr60 δH and Tyr60 εH are the only protons in fast exchange under these conditions. The chemical shifts

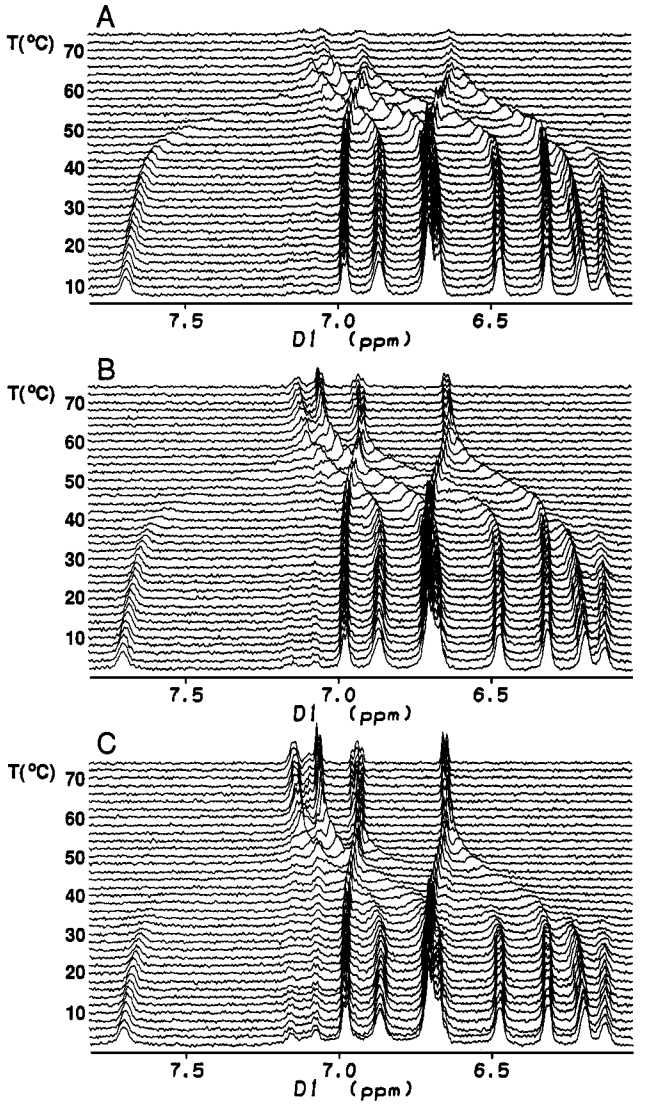

FIGURE 3: Thermal denaturation of 100 μM λ_{6-85} in 20 mM KD_2PO_4, 100 mM NaCl, 17 μg/mL TMSP, and 1 mM NaN_3, pH 8.0, in ~99% D_2O at three urea concentrations, 0 M (A), 1 M (B), and 2 M (C), monitored by ^{1}H NMR of aromatic side chains. Each panel is a stack plot of a series of NMR spectra collected at 2 °C intervals. Chemical shifts (in ppm) of aromatic side-chain protons in the native state (0 M urea, 30 °C) are as follows: Tyr22 δH (6.47), Tyr22 ϵH (6.31), Phe51 δH (6.68), Phe51 ϵH (6.25), Phe51 ζH (6.14), Tyr60 δH (6.97), Tyr60 ϵH (6.70), Phe76 δH (6.70), Phe76 ϵH (6.85), and Phe76 ζH (7.63).

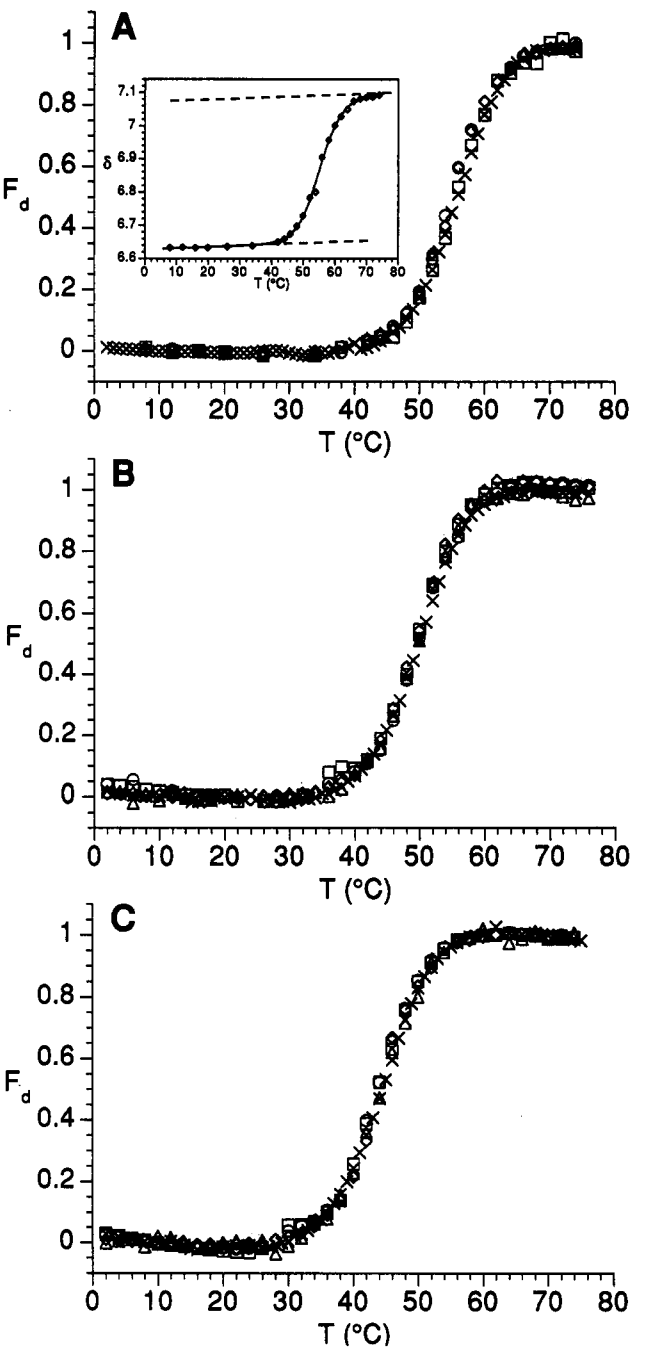

FIGURE 4: Plots of F_d versus temperature derived from NMR (Figure 3) and CD (data not shown) experiments at three urea concentrations, 0 M (A), 1 M (B), and 2 M (C), calculated as described in the text. For clarity, the F_d values of all protons in a residue were averaged to give the F_d shown. The five denaturation curves are indicated by the following symbols: (×) CD signal, (◇) Tyr22, (△) Phe51, (□) Tyr60, and (○) Phe76. The inset in panel A shows an example of the raw data (for Tyr22 δH at 0 M urea), along with the baselines derived from least squares fitting to eqs 1 and 2 (see text).

of these protons were fitted to eqs 3 and 4. Urea denaturation was also monitored by CD at 222 nm and fitted to eqs 3 and 4. The fitted parameters are listed in Table 1. Plots of F_d vs urea from both NMR and CD data are shown in Figure 5. Again, the denaturation curves are superimposable. The fits to eqs 3 and 4 give an average ΔG_0 of 3 ± 0.3 kcal mol^{-1} and an m value of 1.2 ± 0.1 kcal mol^{-1} M^{-1} at 37 °C. These values are reasonable for a stable 80-residue protein (Alonso & Dill, 1991).

DISCUSSION

Comparison of λ_{6-85} to λ_{1-92} and λ_{1-102}. We have investigated the structure and folding of a truncated version of the amino-terminal domain of λ repressor, comprising residues 6−85. This truncated version, which lacks the dimerization interface, is monomeric as judged by the concentration dependence of the 1D ^{1}H NMR spectrum and size exclusion chromatography. There is no evidence of the line broadening observed for λ_{1-102} (Weiss et al., 1987a,b). This makes λ_{6-85} preferable for NMR studies.

In addition to the fact that we characterized the protein in solution, there are several reasons to expect that the structure of λ_{6-85} might differ from the same region in the λ_{1-92}−DNA cocrystal structure. The truncated version is monomeric instead of dimeric, free of DNA, and shorter at the N- and C-termini by 5 and 7 residues, respectively. How-

Table 1: Fitted Parameters Obtained for Nonlinear Least Squares Fits to Raw Urea Denaturation Curves, As Described in the Text

	parameter value[a]					
signal	*a*	*b*	*c*	*d*	ΔG_0	*m*
CD	-79.3 ± 0.2	1.6 ± 0.4	-22.1 ± 0.7	1.0 ± 0.1	3.27 ± 0.08	1.23 ± 0.02
Tyr60 δ	7.14 ± 0.01	1 ± 2	7.11 ± 0.01	-1.7 ± 0.7	2.7 ± 0.4	1.1 ± 0.2
Tyr60 ϵ	6.87 ± 0.01	0 ± 1	6.83 ± 0.01	-1.5 ± 0.5	3.1 ± 0.3	$1.2 \bullet 0.1$

[a] Parameter units: *a* and *c*, mdeg (CD) and ppm (NMR); *b* and *d*, mdeg/M (CD) and ppb/M (NMR); ΔG_0, kcal mol^{-1}; *m*, kcal mol^{-1} M^{-1}.

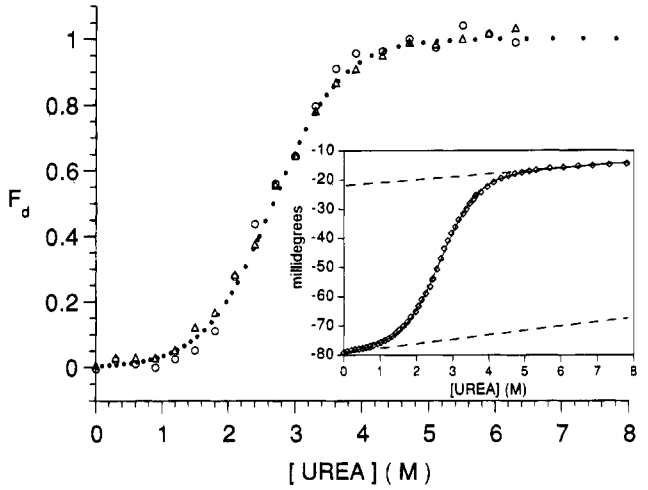

FIGURE 5: Urea denaturation of 50 μM λ_{6-85} in ~99% D_2O, 10 mM CD_3COOD, 100 mM NaCl, 17 μg/mL TMSP, and 1 mM NaN_3, pH 5.6. Plots of F_d versus urea are from the chemical shifts of the Tyr60 aromatic resonances and CD calculated as described in the text. The three denaturation curves are indicated by the following symbols: (•) CD signal, (△) Tyr60 δH, and (○) Tyr60 ϵH. The inset shows the raw CD signal at 222 nm and the fits to eqs 3 and 4 (see text).

ever, several lines of evidence suggest that the solution structure of λ_{6-85} is remarkably similar to the crystal structure of the DNA-bound longer version. First, the T_m of λ_{6-85} (~55 °C) is very close to that of λ_{1-102} (55.7 °C) at ~2 μM, where the longer version is monomeric (Lim et al., 1992). Second, the 11 previously assigned resonances in λ_{1-102} (δCH_3 of L18 and the 10 aromatic resonances) are within 0.1 ppm of those found in λ_{6-85} (Weiss & Hoch, 1987; Weiss et al., 1987a). Third, the short- and mid-range NOEs, protection factors, chemical shift indices, and coupling constants indicate that the secondary structure of λ_{6-85} is identical to that of λ_{1-92}–DNA, although the truncated fifth helix may be unraveling at the C-terminal three residues. Fourth, NOEs for 30 pairs of protons distributed over the entire molecule (Figure 1) are consistent with distances derived from the crystal structure.

Our results are consistent with previous structural studies that detected no major conformational change between the solution structure and crystal structure (Sauer et al., 1990; Weiss et al., 1987a). Similarity between the truncated monomer and the DNA-bound dimer also implies that neither dimerization nor DNA binding introduces any major conformational change, consistent with comparison of the low-resolution crystal structure of the uncomplexed protein (Pabo & Lewis, 1982; Sauer et al., 1990) to the DNA-bound dimer.

Folding of λ_{6-85} Is Two State. Chemical shifts provide a powerful tool for detecting partially folded states under equilibrium (Frieden et al., 1993). If partially denatured species are present, even at low populations, some regions of the protein would be native and others denatured, leading to different local denaturation curves. The ability to discriminate differences in the midpoints of the local denaturation curves determines the sensitivity of the method. For λ_{6-85}, the NMR denaturation curves shown in Figures 4 and 5 have midpoints within 1 °C and 0.1 M urea, respectively, and are superimposable, indicating that the denatured populations (F_d) are identical for all four aromatic residues throughout denaturation. Specifically, the change in population upon exposure of the hydrophobic core (Phe51 ϵH) is identical to the change in population of solvent-exposed protons (Tyr60), which are identical to the population change of partially exposed residues (Tyr22 and Phe76). There is no local unfolding under partially denaturing conditions, and no equilibrium intermediates are observed. These observations hold for thermal denaturation at three urea concentrations and urea denaturation at 37 °C, indicating that two-state behavior results from both methods of denaturation.

Figures 4 and 5 also show that the denaturation curves detected by CD and NMR are superimposable. Coincidence of the CD and NMR data indicates that global unfolding of the secondary structure is identical to localized unfolding of tertiary structure. This observation shows that molten globule (Kuwajima, 1989; Ptitsyn, 1987) or compact denatured states (Flanagan et al., 1992) are not populated in the folding of λ_{6-85}. Taken together, the NMR and CD data indicate that the folding of λ_{6-85} is two state at all temperatures and denaturant concentrations examined. The use of several local probes as well as different physical methods represents a stringent test for two-state folding. As mentioned before, this conclusion will greatly simplify the interpretation of future denaturation experiments, especially kinetic studies.

The approach we have applied in this study allows us to detect populated folding intermediates ("equilibrium intermediates"). We cannot detect short-lived intermediates ("kinetic intermediates") that have populations below ~1%. We also cannot formally exclude the possibility that there are a large number of sparsely populated intermediates with a significant total population. When we describe the folding of λ_{6-85} as two state, we mean that the native and denatured states represent the only significantly populated (>1%) species at all positions on the denaturation curve.

We observe folding of λ_{6-85} in the one-dimensional ^1H NMR spectrum of aromatic side-chain protons without modification of the protein. Aromatic residues are often good probes of structure because they are frequently part of the hydrophobic core and because denaturation exposes the hydrophobic core, often causing large chemical shift changes. In addition, the dispersion of random-coil chemical shifts for the protons of aromatic amino acids makes it possible to follow the chemical shift in a 1D spectrum throughout the denaturation curve, even when the population of unfolded protein is high. This is not usually true for other regions of

the spectrum, which are too crowded to assign in the denatured state by 1D methods. To obtain information about the denatured state using these resonances, higher dimensionality heteronuclear NMR is required (Logan et al., 1994; Neri et al., 1992; Shortle & Abeygunawardana, 1993; Wüthrich, 1994). Nevertheless, the aromatic region of the λ_{6-85} spectrum provides a well-resolved picture of the denaturation throughout the protein.

The magnitude of denaturant-induced chemical shift changes ($\Delta\delta$) provides insight about the structure of the native and denatured states. Phe51 ϵH, Phe51 ζH, and Phe76 ζH exhibit the largest $\Delta\delta$, indicating a dramatic change in the solvent exposure of these groups during denaturation. In the crystal structure, these protons are buried in the hydrophobic core (Figure 1). The denatured state chemical shifts are close to the random-coil values, showing that the hydrophobic core is fully exposed to the solvent upon denaturation. Phe76 δH, Phe76 ϵH, Phe51 δH, Tyr22 δH, and Tyr22 ϵH exhibit intermediate $\Delta\delta$, consistent with their greater solvent exposure to the native structure. In the native state, the side chain of Tyr60 is exposed to solvent. Because this side chain remains accessible to solvent during denaturation, its protons have quite small $\Delta\delta$. The fact that the protons investigated move to "random-coil" positions (Bundi & Wüthrich, 1979) indicates that the denatured state of λ_{6-85} is highly disordered and that the average environment of the aromatic side chains in the denatured state is similar to that of the model tetrapeptides on which the random-coil values are based. The temperature and urea dependence of the chemical shifts is very small in the denatured state, making it unlikely that residual structure in the hydrophobic core is present when F_d is >0.99. These observations support the conclusion that folding of λ_{6-85} is strictly two state.

Folding Time Scale. Under the conditions used here, the folding and unfolding of λ_{6-85} is fast to intermediate on the time scale of the observed NMR resonances, which is determined by $\Delta\delta$. The range of $\Delta\delta$ in λ_{6-85} is 50 Hz (Tyr60 δH) to 600 Hz (Phe51 ζH), giving a time scale of 0.3−3 ms. Because line broadening is observed for the resonances with the largest $\Delta\delta$ values but not for the ones with small $\Delta\delta$ values, the folding of λ_{6-85} is within this range. Future studies to perform detailed line-shape analysis of resonances in intermediate exchange should allow accurate measurement of the folding rate (G. S. Huang and T. G. Oas, unpublished experiments). In the current study, we have exploited fast−intermediate exchange to use chemical shift as a probe of folding. Most proteins fold in the slow exchange regime, where folding rates are much slower than chemical shift differences and separate peaks are usually observed for each species (Roder, 1989). The relative populations can be deduced from the intensities of the corresponding peaks (Westmoreland & Matthews, 1973; Dobson et al., 1985). However, chemical shift can be measured more precisely than peak intensities or integrals. Futhermore, chemical shifts can be precisely measured even with very dilute samples.

CONCLUSIONS

The powerful tools of multidimensional heteronuclear NMR have made it possible to assign and obtain structural information for the denatured states of proteins (Logan et al., 1994; Neri et al., 1992; Shortle & Abeygunawardana, 1993; Wüthrich, 1994). However, to assess the thermodynamic relevance of these denatured states, it is critical to determine relative populations of the various species present under denaturing conditions. Here, we present a new method, demonstrated with 1D NMR but readily extendable to heteronuclear methods, for detecting equilibrium protein folding intermediates. To demonstrate the method, we have used a truncated version of the amino-terminal fragment of λ repressor (λ_{6-85}) which folds in a stable conformation very similar in structure to the dimer−DNA complex. We have applied ^{1}H NMR as a local probe and CD as a global probe to monitor the denaturation. By both thermal and urea denaturation, local structural changes are identical to the global change detected by CD. Therefore, the denaturation of this protein is a two-state process. This study has led to a rigorous method for establishing two-state behavior which could also be applied to other fast-folding proteins.

ACKNOWLEDGMENT

We thank Wendell Lim for sharing the λ_{6-85} construct and for his inspiration of this project, Ron Venters of the Duke NMR Center for assistance with NMR experiments, Margaret Daugherty for many helpful discussions, Tiffany Calderone for technical assistance, and Gary Pielak, Eric Toone, Neil Tweedy, and Carol Fierke for their comments on the manuscript.

SUPPLEMENTARY MATERIAL AVAILABLE

Table 1 listing ^{1}H, ^{15}N, and backbone ^{13}C chemical shift assignments for λ_{6-85} and Table 2 listing the parameters used to fit the thermal denaturation curves (6 pages). Ordering information is given on any current masthead page.

REFERENCES

Alonso, D. O., & Dill, K. A. (1991) *Biochemistry 30*, 5974−5985.
Bai, Y., Milne, J. S., Mayne, L., & Englander, S. W. (1993) *Proteins: Struct., Funct., Genet. 17*, 75−86.
Bax, A., & Subramanian, S. (1986) *J. Magn. Reson. 67*, 565−569.
Beamer, L. J., & Pabo, C. O. (1992) *J. Mol. Biol. 227*, 177−96.
Braunschweiler, L., & Ernst, R. R. (1983) *J. Magn. Reson. 53*, 521.
Bundi, A., & Wüthrich, K. (1979) *Biopolymers 18*, 285−298.
Creighton, T. E. (1993) *Proteins: Structures and Molecular Principles*, 2nd ed., W. H. Freeman, New York.
Davis, D. G., & Bax, A. (1985) *J. Am. Chem. Soc. 107*, 2820−2821.
de Marco, A. (1977) *J. Magn. Reson. 26*, 527−528.
Dill, K. A., & Shortle, D. (1991) *Annu. Rev. Biochem. 60*, 795−825.
Dobson, C. M., Evans, P. A., & Fox, R. O. (1985) in *Structure & Motion: Membranes, Nucleic Acids and Proteins* (Clementi, E., Corongiu, G., Sarma, M. H., & Sarma, R. H., Eds.) pp 265−275, Adenine Press, New York.
Doering, D. S. (1992) Ph.D. Thesis, Massachusetts Institute of Technology.
Eliason, J. L., Weiss, M. A., & Ptashne, M. (1985) *Proc. Natl. Acad. Sci. U.S.A. 82*, 2339−2343.
Englander, S. W., Downer, N. W., & Teitelbaum, H. (1972) *Annu. Rev. Biochem. 41*, 903−924.
Farmer, B. T., II, Venters, R. A., Spicer, L. D., Wittekind, M. G., & Müler, L. (1992) *J. Biomol. NMR 2*, 195−202.
Flanagan, J. M., Kataoka, M., Shortle, D., & Engelman, D. M. (1992) *Proc. Natl. Acad. Sci. U.S.A. 89*, 748−752.
Forman-Kay, J. D., Gronenborn, A. M., Kay, L. E., Wingfield, P. T., & Clore, G. M. (1990) *Biochemistry 29*, 1566−1572.
Frieden, C., Hoeltzli, S. D., & Ropson, I. J. (1993) *Protein Sci. 2*, 2007−2014.
Gronenborn, A. M., Bax, A., Wingfield, P. T., & Clore, G. M. (1989) *FEBS Lett. 243*, 93−98.

Ikura, M., Kay, L. E., & Bax, A. (1990) *Biochemistry 29*, 4659–4667.
Jackson, S. E., & Fersht, A. R. (1991) *Biochemistry 30*, 10428–10435.
Jordan, S. R., & Pabo, C. O. (1988) *Science 242*, 893–899.
Kraulis, P. K. (1991) *J. Appl. Crystallogr. 24*, 946–950.
Kuwajima, K. (1989) *Proteins 6*, 87–103.
Lattman, E. E., & Rose, G. D. (1993) *Proc. Natl. Acad. Sci. U.S.A. 90*, 439–441.
Levy, G. C., & Lichter, R. L. (1979) *Nitrogen-15 Nuclear Magnetic Resonance Spectroscopy*, J. Wiley & Sons, New York.
Lim, W. A., & Sauer, R. T. (1989) *Nature 339*, 31–36.
Lim, W. A., & Sauer, R. T. (1991) *J. Mol. Biol. 219*, 359–376.
Lim, W. A., Farruggio, D. C., & Sauer, R. T. (1992) *Biochemistry 31*, 4324–4333.
Logan, T. M., Theriault, Y., & Fesik, S. W. (1994) *J. Mol. Biol. 236*, 637–648.
Macura, S., & Ernst, R. R. (1980) *Mol. Phys. 41*, 95.
Murphy, K. P., Bhakuni, V., Xie, D., & Freire, E. (1992) *J. Mol. Biol. 227*, 293–306.
Neri, D., Wider, G., & Wüthrich, K. (1992) *FEBS Lett. 303*, 129–135.
Pabo, C. O., & Lewis, M. (1982) *Nature 298*, 443–447.
Pace, C. N. (1986) *Methods Enzymol. 131*, 266–280.
Powers, R., Garrett, D. S., March, C. J., Frieden, E. A., Gronenborn, A. M., & Clore, G. M. (1992) *Biochemistry 31*, 4334–4346.
Privalov, P. L., & Khechinashvili, N. N. (1974) *J. Mol. Biol. 86*, 665–684.
Ptitsyn, O. B. (1987) *J. Protein Chem. 6*, 273–293.
Rance, M., Sorensen, O. W., Bodenhausen, G., Wagner, G., Ernst, R. R., & Wüthrich, K. (1983) *Biochem. Biophys. Res. Commun. 117*, 479–485.
Reidhaar-Olson, J. F., & Sauer, R. T. (1990) *Proteins 7*, 306–316.
Roder, H. (1989) *Methods Enzymol. 176*, 446–473.
Sauer, R. T., Jordan, S. R., & Pabo, C. O. (1990) *Adv. Protein Chem. 40*, 1–61.
Schellman, J. (1987) *Annu. Rev. Biophys. Biophys. Chem. 16*, 115–137.
Schellman, J. A. (1994) *Biopolymers 34*, 1015–1026.
Shaka, A. J., & Freeman, R. (1983) *J. Magn. Reson. 51*, 169.
Shortle, D., & Abeygunawardana, C. (1993) *Structure 1*, 121–134.
States, D. J., Haberkorn, R. A., & Ruben, D. J. (1981) *J. Magn. Reson. 48*, 286–292.
Studier, F. W., Rosenberg, A. H., Dunn, J. J., & Dubendorff, J. W. (1990) *Methods Enzymol. 185*, 60–89.
Vuister, G. W., Boelens, R., Kaptein, R., Burgering, M., & van Zijl, P. C. M. (1992) *J. Biomol. NMR 2*, 301–305.
Weiss, M. A., & Hoch, J. C. (1987) *J. Magn. Reson. 72*, 324–333.
Weiss, M. A., Sauer, R. T., Patel, D. J., & Karplus, M. (1984) *Biochemistry 23*, 5090–5095.
Weiss, M. A., Karplus, M., & Sauer, R. T. (1987a) *Biochemistry 26*, 890–897.
Weiss, M. A., Pabo, C. O., Karplus, M., & Sauer, R. T. (1987b) *Biochemistry 26*, 897–904.
Wemmer, D., Ribeiro, A. A., Bray, R. P., Wade, J. N., & Jardetzky, O. (1981) *Biochemistry 20*, 829–833.
Westmoreland, D. G., & Matthews, C. R. (1973) *Proc. Natl. Acad. Sci. U.S.A. 70*, 914–918.
Wishart, D. S., Sykes, B. D., & Richards, F. M. (1991) *J. Mol. Biol. 222*, 311–333.
Wishart, D. S., Sykes, B. D., & Richards, F. M. (1992) *Biochemistry 31*, 1647–1651.
Wüthrich, K. (1986) *NMR of Proteins and Amino Acids*, Wiley, New York.
Wüthrich, K. (1994) *Cur. Opin. Struct. Biol. 4*, 93–99.

BI950137F